Chelator sensing and lipopeptide interplay mediates molecular interspecies interactions between soil bacilli and pseudomonads

Sofija Andric´[1*], Thibault Meyer[1,2*], Augustin Rigolet[1], Anthony Argüelles Arias[1], Sébastien Steels[1], Grégory Hoff[1#], Monica Höfte[3], René De Mot[4], Andrea McCann[5], Edwin De Pauw[5] and Marc Ongena[1]

[1]Microbial Processes and Interactions Laboratory, Terra Teaching and Research Center, Gembloux Agro-Bio Tech, University of Liège, Gembloux, Belgium

[2]UMR Ecologie Microbienne, F-69622, University of Lyon, Université Claude Bernard Lyon 1, CNRS, INRAE, VetAgro Sup, Villeurbanne, France

[3]Laboratory of Phytopathology, Department of Plants and Crops, Faculty of Bioscience engineering, Ghent University, Gent, Belgium

[4] Centre of Microbial and Plant Genetics, Faculty of Bioscience Engineering, University of Leuven, Heverlee, Belgium

[5] Mass Spectrometry Laboratory, , MolSys Research Unit, Department of Chemistry, University of Liège, Belgium

[#]Current address: Ecology and Biodiversity, Department of Biology, Utrecht University, Padualaan 8, 3584 CH, Utrecht, The Netherlands

* Equal contribution

Abstract

Some bacterial species are important members of the rhizosphere microbiome and confer protection to the host plant against pathogens. However, our knowledge is still limited about the multitrophic interactions determining the ecological fitness of these biocontrol bacteria in their highly competitive natural niche. In

this work, we have investigated the molecular mechanisms underlying interactions between *B. velezensis,* considered as model plant-associated and beneficial species in the *Bacillus* genus, and *Pseudomonas* as a rhizosphere-dwelling competitor. Our data show that *B. velezensis* boosts its arsenal of specialized antibacterials upon the perception of the secondary siderophore pyochelin produced by phylogenetically distinct pseudomonads and some other genera. We postulate that *B. velezensis* has developed some chelator sensing systems to learn about the identity of its surrounding competitors. Illustrating the multifaceted molecular response of *Bacillus*, surfactin is another crucial component of the secondary metabolome mobilized in interbacteria competition. Its accumulation not only enhances motility capability but, unexpectedly, this lipopeptide also acts as a chemical trap that reduce the toxicity of other lipopeptides released by *Pseudomonas* challengers. This favors the persistence of *Bacillus* populations upon competitive root colonization. Our work thus highlights new ecological roles for bacterial secondary metabolites acting as key drivers of social interactions.

INTRODUCTION

Soil is one of the richest ecosystems in terms of microbial diversity and abundance[1]. However, the scarcity of resources makes it one of the most privileged environment for competitive interspecies interactions [2,3]. A subset of the bulk soil microbes has evolved to dwell in the rhizosphere compartment surrounding roots due to continued nutrient-enriched exudation from the plant. Compared to bulk soil, microbial warfare in the rhizosphere is presumably even more intense as the habitat is spatially restricted and more densely populated[3]. Besides rivalry for nutrients (exploitative), interference competition is considered as a key factor driving microbial interactions and community assembly. It can involve signal interference or toxins deployed by contact-dependent delivery systems[4,5] but is mainly mediated at distance through the emission of various molecular weapons. The molecular basis of interference interactions and their phenotypic outcomes between diverse soil bacterial species have been amply investigated in the last decade[6,7].

Like some genera of the Proteobacteria, Actinobacteria, and Bacteroidetes taxa, bacilli belonging to the *B. subtilis* complex are ubiquitous members of the rhizosphere microbiome[2,8,9]. Among these species, *B. velezensis* has emerged as a model for plant-associated bacilli and displays strong potential as biocontrol agents reducing diseases caused by phytopathogens[10]. *B. velezensis* distinguish from other species of the *B. subtilis* group regarding their richness in biosynthetic gene clusters (BGCs, representing up to 13% of the

whole genome) responsible for the synthesis of bioactive secondary metabolites (BSMs) [11,12]. This chemically-diverse secondary metabolome includes volatiles, terpenes, non-ribosomal (NR) dipeptides, cyclic lipopeptides (CLPs) and polyketides (PKs), but also ribosomally synthesized lantibiotics and larger bacteriocins (RiPP) [13,14]. BSMs are involved in the biocontrol activity via direct inhibition of infectious microbes and/or via stimulation of the plant immune system[15,16]. From an ecological viewpoint, BSMs also contribute to competitiveness in the rhizosphere niche thanks to multiple and complementary functions as drivers of developmental traits, as antimicrobials, or as signals initiating cross-talk with the host plant[17–19 20–26].

Mostly guided by practical concerns for use as biocontrol agents, research on BSMs has mainly focused on the characterization of their biological activities. However, the impact of environmental factors that may modulate their expression under natural conditions has been much poorly investigated. It includes interactions with other organisms sharing the niche. Some recent reports illustrate how soil bacilli may adapt their behavior upon sensing bacterial competitors but almost exclusively focusing on developmental traits (sporulation, biofilm formation, or motility)[6]. Unlike other genera such as *Streptomyces*, it remains largely unknown to what extent bacilli in general and *B. velezensis* in particular, may modulate the expression of their secondary metabolome upon interaction with other bacteria[2,8,9,27]. Through this work, we wanted to investigate the molecular outcomes of interspecies interactions that *B. velezensis* may engage. We selected *Pseudomonas* as challenger considering that species of this genus are also highly competitive and commonly encountered in rhizosphere microbiomes[8]. We performed experiments under nutritional conditions mimicking the oligotrophic rhizosphere environment and used contact-independent settings for pairwise interaction which also obviously best reflect the real situation in the soil. Our data revealed that the two bacteria initiate a multifaceted interactions mostly mediated by the non-ribosomally synthesized components of their secondary metabolome. We pointed out unsuspected roles for some of these BSMs in the interaction context. Beyond its role as a metal chelator, the *Pseudomonas* secondary siderophore pyochelin acts as a signal triggering dual production of PKs and RiPP in *Bacillus* while specific lipopeptides modulate the inhibitory interaction between the two species. This resulted in marked phenotypic changes in *B. velezensis* such as higher antibacterial potential, enhanced motility and protective effect via chemical trapping. We also illustrate the relevance of these outcomes in the context of competitive root colonization.

RESULTS

B. velezensis modulates its secondary metabolome and boosts antibacterial activity upon sensing *Pseudomonas* metabolites

In this study, we used *B. velezensis* strain GA1 as BSM-rich and genetically amenable isolate representative of the species. Genome mining with AntiSMASH 5.0 [28] confirmed the presence of all gene clusters necessary for the biosynthesis of diverse known BSMs typically formed by this bacterium (Supplementary Table 1). Based on the exact mass and absence of the corresponding peaks in deletion mutants, most of the predicted non-ribosomal (NR) secondary metabolites were identified in cell-free crude supernatants via optimized UPLC-MS (Supplementary Fig. 1). It includes the whole set of cyclic lipopeptides (CLPs of the surfactin, fengycin and iturin families) and polyketides (the PKs difficidin, macrolactin and bacillaene) with their multiple co-produced structural variants, as well as the siderophore bacillibactin. We verified that all these compounds are readily formed in the so-called exudate-mimicking (EM) medium reflecting the specific content in major carbon sources typically released by roots of Solanaceae (such as tomato) plants[29]. In addition to these NR products, genes encoding RiPPs such as amylocyclicin and amylolysin are also present in GA1 but these compounds could not be reliably detected in culture broths. The NR dipeptide bacilysin was also predicted but not detected. We selected as the main interaction partner the plant-associated *Pseudomonas* sp. strain CMR12a based on its biocontrol potential and its production of multiple secondary metabolites [30–34]. Genome mining confirmed the potential of CMR12a to synthesize a range of BSMs, including antimicrobial phenazines, the siderophores pyoverdin (structure confirmation in Supplementary Fig. 2) and (enantio-)pyochelin as well as two structurally distinct CLPs, sessilin and orfamide (Supplementary Table 1). In contrast to *Bacillus*, the capacity to co-produce two different CLPs is a quite rare trait for non-phytopathogenic pseudomonads and represented an additional criterion for selecting strain CMR12a for this study[30,34–36]. In the case of CMR12a, all these compounds were detected in EM culture broth but most of them are more efficiently produced upon growth in Casamino Acids medium (CAA) commonly used for *Pseudomonas* cultivation (Supplementary Fig. 1).

Our prime objective was to evaluate the intrinsic potential of *B. velezensis* to react to the perception of *Pseudomonas* metabolites in an experimental setting avoiding interferences due to diffusion constraints in a semi-solid matrix or due to the formation of impermeable biofilm structures. The first assays were performed by growing GA1 in agitated liquid EM medium supplemented or not with (sterile) BSM-containing spent medium of CAA-grown CMR12a (CFS, cell-free supernatant). At low dose (2% (v/v)), the

addition of this CFS extract led to a marked increase in the production of some GA1 NR metabolites. Significantly higher amounts were measured for surfactin, bacillaene and its dehydrated variant, difficidin and its oxidized form, and bacillibactin (Fig. 1a, b) but not for fengycin, iturin nor macrolactin (Fig 1a).

Such boost in BSM synthesis triggered by *Pseudomonas* CFS was associated with an increase in the antibacterial activity of the corresponding extracts when tested for growth inhibition of *Xanthomonas campestris* and *Clavibacter michiganensis* used respectively as representative of Gram-negative and Gram-positive plant pathogenic bacteria of agronomical importance[37] (Fig. 1c). Since most of the BSMs are not commercially available and our attempt to purify PKs failed due to chemical instability, we could not use individual compounds for their specific involvement in bacterial inhibition. As an alternative, we generated and tested a range of GA1 knockout mutants including the Δ*sfp* derivative specifically repressed in 4'-phosphopantetheinyl transferase essential for the proper functioning of the PK and NRP biosynthesis machinery. Full loss of anti-*Xanthomonas* activity in Δ*sfp* extracts indicated a key role for NR BSMs and ruled out the possible involvement of other chemicals known for their antibacterial activity such as bacilysin or RiPPs (Fig. 1d). Loss of function of mutants specifically repressed in the synthesis of individual compounds pointed out the key role of (oxy)difficidin and to a lower extent of (dihydro)bacillaene in *Xanthomonas* inhibition (Fig. 1d). These two polyketides are also responsible for GA1 inhibitory activity toward other important bacterial phytopathogens such as *Pectobacterium carotovorum*, *Agrobacterium tumefaciens* and *Rhodococcus fasciens* but are not involved in the inhibition of plant pathogenic *Pseudomonas* species for which bacilysin may be the active metabolite (Supplementary Fig. 3). However, as illustrated below in the next sections, *B. velezensis* does not display significant toxicity against CMR12a and other non-pathogenic soil *Pseudomonas* isolates tested here. Stimulation of PKs synthesis upon sensing CMR12a is not specific to GA1 and was also observed in other *B. velezensis* strains such as S499, FZB42 and QST713 with well-known biocontrol potential[38–40] (Supplementary Fig. 4).

In contrast to *Xanthomonas*, the enhanced antibiotic activity against *Clavibacter* is not mediated by NR products as shown by the fully conserved activity in the Δ*sfp* mutant (Fig. 1d). We, therefore, suspected from genomic data that some RiPPs such as amylocyclicin could be involved in inhibition. This hypothesis was supported by the 80% reduction in antibiotic potential observed for the Δ*acnA* mutant knocked out for the corresponding biosynthesis gene (Fig. 1d). Besides, RT-qPCR data revealed a highly induced expression of the *acnA* in GA1 cells upon supplementation with CMR12a CFS (Fig. 1e) but we were not able to provide

143 evidence for higher accumulation of the mature peptide in the medium. Enhanced expression of the *acnA*
144 gene in presence of *Pseudomonas* products was also observed for strain S499 (Supplementary Fig. 5).

145 **Pyochelin acts as a signal sensed by *Bacillus* to stimulate polyketide production**

146 We next wanted to identify the signaling molecules secreted by *Pseudomonas* that are sensed by *Bacillus*
147 cells and lead to improved BSMs production. For that purpose, we used dihydrobacillaene (2H-bae) as an
148 indicator of the *Bacillus* response because it represents the most consistent and highly boosted polyketide
149 species. We first compared the triggering potential of CFS obtained from knockout mutants of CMR12a
150 specifically lacking the different metabolites identified (Supplementary Fig. 1). Only extracts from mutants
151 impaired in the production of siderophores and more specifically pyochelin were significantly affected in
152 PKs-inducing potential (Fig. 2a). Possible involvement of this compound was supported by the drastic
153 reduction in the activity of CFS prepared from CMR12a culture in CAA medium supplemented with Fe^{3+}
154 where siderophore expression is repressed (Supplementary Fig. 6). We also performed bioactivity-guided
155 fractionation and data showed that only extracts containing pyoverdine and/or pyochelin displayed
156 consistent PKs-triggering activity (Supplementary Fig. 7). HPLC-purified compounds were also tested
157 independently at a concentration similar to the one used in CFS CAA extract and it revealed a much higher
158 PK-triggering activity for pyochelin compared to the main pyoverdine isoform (Fig. 2b). Dose-dependent
159 assays further indicated that supplementation with pyoverdine, as strong chelator[41], caused some iron
160 limitation in the medium which is sensed by GA1. It is reflected first by the marked increase in production of
161 the siderophore bacillibactin in GA1 wild-type (Fig. 2c) and by the reduced growth of a Δ*dhbC* mutant
162 repressed in bacillibactin synthesis upon pyoverdin addition (Fig. 2d, Supplementary Fig. 8 for statistics).
163 This last result indicates that pyoverdine in its ferric form cannot be taken up by GA1 despite the presence
164 of several transporters for exogenous siderophores in *B. velezensis* similar to those identified in *B.*
165 *subtilis*[42,43] based on genome comparison (Supplementary Table 2). We, therefore, assumed that iron stress
166 mediated by pyoverdine only induces a rather limited boost in PKs production. We validate that such
167 response is not due to iron starvation by supplementing GA1 culture with increasing doses of the 2,2'-
168 dipyridyl chemical chelator that cannot be taken up by Bacillus cells (Fig. 2b). By contrast, the addition of
169 pyochelin with a much lower affinity for iron does not activate bacillibactin synthesis (Fig. 2c) and does not
170 affect Δ*dhbC* growth at the concentrations used (Fig. 2d). We concluded that the activity of this compound
171 referred to as secondary siderophore is not related to iron-stress. If internalized, pyochelin can cause
172 oxidative stress and damage in other bacteria as reported for *E. coli* [44,45] . However, the absence of toxicity

toward GA1 indicates that pyochelin is not taken up by *Bacillus* cells and thus clearly acts as a signal molecule perceived at the cell surface. PKS boost also occurred upon addition of CFS obtained from other *Pseudomonas* isolates such as *P. protegens* Pf-5[46] and *P. aeruginosa* PAO1 [47] producing pyochelin-type siderophores. However, PKS stimulation was also observed in response to *P. tolaasi* CH36[48] and *Pseudomonas* sp. A214[49] that do not form pyochelin indicating that some other unidentified BSMs may act as triggers in other strains (Supplementary Figure 9).

Enhanced motility as distance-dependent and surfactin-mediated response of *Bacillus*

Surfactin production is also stimulated by CMR12a CFS and by pure pyochelin (Fig. 1a and Supplementary Fig. 10). Based on the mutant analysis, this multifunctional CLP does not contribute to the antibacterial potential of *B. velezensis* (Fig 1d and Supplementary Fig. 3) but is notably involved in developmental processes of multicellular communities such as biofilm formation and motility[50]. We, therefore, wanted to test a possible impact of *Pseudomonas* on the motile phenotype of *B. velezensis* upon co-cultivation on plates. We observed distance-dependent enhanced motility on gelified medium containing high agar concentrations (1.5% m/v) which phenotypically resembles the sliding-type of motility illustrated by typical "van Gogh bundles"[50] (Fig. 3a). This migration pattern is flagellum independent but depends on multiple factors including the synthesis of surfactin which reduces friction at the cell-substrate interface[50]. We thus suspected such enhanced motility to derive from an increased formation of the lipopeptide. This was supported by the almost full loss of migration of the Δ*srfaA* mutant in these interaction conditions (Fig. 3b). Moreover, spatial mapping via Maldi-FT-ICR MS imaging confirmed a higher accumulation of surfactin ions in the interaction zone and around the *Bacillus* colony when it is growing at a short or intermediate distance from the *Pseudomonas* challenger compared to the largest distance where the motile phenotype is much less visible (Fig. 3c). These data indicate that *Bacillus* cells in the microcolony perceive some soluble signal diffusing from the *Pseudomonas* colony to a limited distance.

Interplay between CLPs drives antagonistic interactions

Furthermore, we observed that, besides modulating secondary metabolite synthesis, confrontation with *Pseudomonas* may also lead to some antagonistic outcomes. GA1 growth as planktonic cells is slightly inhibited upon supplementation of the medium with 2% v/v CMR12a CFS but this inhibition is much marked at higher doses (Supplementary Fig. 11). To identify the *Pseudomonas* compound retaining such antibiotic activity, we tested the effect of CFS from various CMR12a mutants impaired in the synthesis of lipopeptides

and/or phenazines. Even if some contribution of other compounds cannot be ruled out, it revealed that the CLP sessilin is mainly responsible for toxic activity toward GA1 grown in liquid cultures but also when the two bacteria are grown at close proximity on gelified EM medium (Fig 4a). Nevertheless, we observed that the sessilin-mediated inhibitory effect is markedly reduced by delaying CFS supplementation at 6h of culture instead of adding at the beginning of incubation (Fig 4b). This suggested that some early secreted *Bacillus* compounds may counteract the toxic effect of sessilin. We hypothesized that surfactin can play this role as it is the first detectable BSM to accumulate in significant amounts in the medium at early growth. We tested the surfactin-deficient mutant in the same conditions and observed that its growth is still strongly affected indicating that no other GA1 compound may be involved in toxicity alleviation. Chemical complementation with purified surfactin allowed to restore growth to a large extent, providing further evidence for a protective role of the surfactin lipopeptide (Fig. 4b). Such sessilin-dependent inhibition also occurred when bacteria were confronted on solid CAA medium favoring *Pseudomonas* BSM production (Fig. 4c-I). In these conditions, the formation of a white precipitate in the interaction zone was observed with CMR12a wild type but not when GA1 was confronted with the Δ*sesA* mutant (Fig. 4c). UPLC-MS analysis of ethanol extracts from this white-line area confirmed the presence of sessilin ions but also revealed an accumulation of surfactin from GA1 in the confrontation zone (Fig. 4d). The involvement of surfactin in precipitate formation was confirmed by the absence of this white-line upon testing the Δ*srfaA* mutant of GA1 (Fig. 4c). The loss of surfactin production and white-line formation was associated with a higher sensitivity of the *Bacillus* colony to the toxin secreted by *Pseudomonas*. Altogether, these data indicate that surfactin acts as a chemical trap and inactivates sessilin via co-aggregation into insoluble complexes.

A similar CLP-dependent antagonistic interaction and white-line formation were observed upon co-cultivation of GA1 with *P. tolaasii* strain CH36 producing tolaasin (Fig. 4c), a CLP structurally very similar to sessilin (only differing by a single amino acid residue, Supplementary Fig. 12). However, this chemical aggregation is quite specific regarding the type of CLP involved since it was not visible upon the interaction of GA1 with other *Pseudomonas* strains forming different CLP structural groups that are not toxic for *Bacillus* (Fig. 4c, see Supplementary Fig. 12 and 13 for identification and structures). Sessilin/tolaasin-dependent toxicity and white-line formation were also observed when other surfactin-producing *B. velezensis* isolates are confronted with CMR12a and CH36 (Supplementary Figs. 14 and 15, respectively). Although the chemical basis and the steochiometry of such molecular interaction remain to be determined, it probably follows the same rules as observed for the association between sessilin/tolaasin and other

endogenous *Pseudomonas* CLPs such as WLIP or orfamide[35] or between CLPs and other unknown metabolites[51,52].

BSM-mediated interactions drive competitive root colonization

Our *in vitro* data thus point out how *B. velezensis* may modulate its secondary metabolome when confronted to *Pseudomonas*. To appreciate the relevance of our findings in a more realistic context, we next evaluated whether such BSM interplay may also occurred upon root co-colonization of tomato plantlets and its possible impact on *Bacillus* fitness. When inoculated independently, CMR12a colonized roots more efficiently than GA1 within the first 5 days, most probably due to a higher intrinsic growth rate[53]. Upon co-inoculation, CMR12a colonization rate was not affected but GA1 populations were reduced compared to mono-inoculated plantlets (Fig. 5a). UPLC-MS analysis of methanolic extracts prepared from co-bacterized roots (and surrounding medium) revealed substantial amounts of pyochelin (Supplementary Fig. 16) indicating that the molecule is readily formed under these conditions and could therefore also act as a signal *in planta.* Probably due to the low populations of GA1, we could not detect Bacillus PKs and RiPPs in these extracts. However, a significantly enhanced expression of gene clusters responsible for the synthesis of bacillaene, difficidin and amylocyclicin was observed in GA1 cells confronted to *Pseudomonas* compared to single inoculation (Fig 5b). It indicated that the metabolite response observed in GA1 cell cultures in EM medium may also occur upon competitive colonization where the bacteria feed exclusively on root exudates.

Lipopeptides involved in the interference interaction described in the previous section are also readily formed upon single and dual root colonization (Fig. 5d). We hypothesized that the inhibitory effect of sessilin may impact the colonization potential of GA1 in presence of CMR12a which was confirmed by the increase in GA1 populations co-inoculated with the Δ*sesA* mutant (Fig 5c). Moreover, colonization by the Δ*srfaA* mutant is more impacted compared to WT when co-cultivated with CMR12a and a significant gain in root establishment is recovered upon co-colonization with the Δ*sesA* mutant (Fig. 5d). The sessilin-surfactin interplay thus also occurs *in planta.* Sessilin would confer a competitive advantage to CMR12a during colonization by inhibiting GA1 development but efficient surfactin production on roots, however, may provide some protection to *Bacillus* cells.

DISCUSSION

Our current knowledge on the molecular interaction between soil bacilli and pseudomonads is rather limited, except the fact that the Type VI secretion system and the antibiotic 2,4-diacetylphloroglucinol may impact key developmental traits in *B. subtilis* such as biofilm formation and/or sporulation rate[54,55]. Here we show that the model species *B. velezensis* can mobilize a substantial part of its secondary metabolome to face *Pseudomonas* competitors. Our data provide the first evidence for the enhanced synthesis of broad-spectrum PKs (bacillaene and difficidin-type acting independently or in synergy) together with stimulation of bacteriocin production in *Bacillus* upon perception of other bacteria both in contact-independent *in vitro* settings and upon competitive root colonization. This correlates with an enhanced antibacterial potential which is of interest for biocontrol but which can also be considered as a defensive strategy to persist in its natural competitive niche. *B. velezensis* calls its antibiotic arsenal upon sensing *Pseudomonas* but we also show that the bacterium also recruits its multifunctional surfactin CLP to improve multicellular mobility. It may represent an escape mechanism enabling *Bacillus* cells to relocate after detecting harmful challengers. Improved motility of *B. subtilis* has been already described upon sensing competitors such as *Streptomyces venezuelae*[6,56] but no relationship was established with enhanced production of BSMs potentially involved in the process. We also highlight a new role for surfactin acting as a chemical shield to counteract the toxicity of exogenous CLPs. Intraspecies CLP co-precipitation has been reported[30] but our results make sense of this phenomenon in the context of interference interaction between two different genera. In planta, this new function of surfactin contributes to *Bacillus* competitiveness for root invasion. This has to be added to other previously reported implications of surfactin in *B. subtilis* interspecies interactions such as interfering with the growth of closely related species in synergy with cannibalism toxins [57], inhibiting the development of *Streptomyces* aerial hyphae [58] or participating in the expansion and motility of the interacting species [59].

Furthermore, we exemplify that PKs stimulation in *B. velezensis* is mainly mediated by pyochelin (even if other secreted products can also play some role) produced by *Pseudomonas* as secondary siderophore. Our data show that *Bacillus* perceives pyochelin in a way independent of iron stress and piracy indicating that beyond its iron-scavenging function, this siderophore may thus also act as infochemical in interspecies cross-talk. In the pairwise system used here, pyochelin signaling superimposes the possible effect of iron limitation in the external medium which may also result in enhanced production of antibacterial metabolites by *Bacillus* as occasionally reported[60]. That said, due to the limitation in bioavailable iron, almost all known rhizobacterial species have adapted to produce their siderophores to compete for this

essential element. Siderophore production is thus probably the most widely conserved trait among soil bacteria. It also means that upon recognition of exogenous siderophores, any isolate may somehow identify surrounding competitors. However, some of these siderophores are structurally very variable and almost strain-specific (such as pyoverdins from fluorescent pseudomonads) while some others are much more widely distributed across species and even genera (enterobactin-like, citrate). In both cases, their recognition would not provide proper information about the producer because too specific or too general respectively. Interestingly, the synthesis of pyochelin and its structurally very close enantio form is conserved in several but not all *Pseudomonas* sp. as well as in a limited number of species belonging to other genera such as *Burkholderia* and *Streptomyces*. We,therefore, hypothesize that *Bacillus* may have evolved some chelator-sensing systems targeting siderophores that are conserved enough to be detected but restricted to specific microbial phylogenetic groups. With this mechanism, soil bacilli would rely on siderophores as public goods to accurately identify competitors and respond in an appropriate way like remodeling its BSM secretome. This novel concept of chelator sensing represents a new facet of the siderophore-mediated social interactions. Whether it is used for other secondary siderophores than pyochelin and if yes whether this adaptative trait can be generalized to other soil-dwelling species remains to be determined.

In summary, we provide the first evidence that the model *B. velezensis* species can mobilize a substantial part of his secondary metabolome upon a perception of *Pseudomonas* competitors. Beyond the notion of specialized metabolites, we point out unsuspected additional functions for some of these small molecules in the context of interactions between bacterial clades that are important members of the plant-associated microbiome. This metabolite response is viewed as a way to mount a multi-faceted defensive strategy to gain fitness and persistence in its natural competitive niche.

MATERIAL AND METHODS

Bacterial strains and growth conditions

Strains and plasmids used in this study are listed in Supplementary Table S1. *B. velezensis* strains were grown on recomposed exudate (EM) solid medium [29] or with shaking (160 rpm), at 30°C in EM liquid medium. Deletion mutants of *B. velezensis* were selected on chloramphenicol (5 µg/ml) and/or phleomycin

(4 µg/ml) on Lysogeny broth (LB) (10 g l^{-1} NaCl, 5 g l^{-1} yeast extract and 10 g l^{-1} tryptone). *Pseudomonas* sp. strains were grown on King B (20 g l^{-1} of bacteriological peptone, 10 g l^{-1} of glycerol and 1.5 g l^{-1} of K_2HPO_4, 1.5 g l^{-1} of $MgSO_4.7H_2O$, pH=7) and casamino acid (CAA) solid and liquid medium (10 g l^{-1} Casamino acid, 0.3 g l^{-1} K_2HPO_4, 0.5 g l^{-1} $MgSO_4$ and pH=7) with shaking (120 rpm), at 30°C. The phytopathogenic bacterial strains were grown on LB and EM solid and liquid media and with shaking (150 rpm), at 30°C.

Construction of deletion mutants of *B. velezensis* GA1

All deletion mutants were constructed by marker replacement. Briefly, 1 kb of the upstream region of the targeted gene, an antibiotic marker (chloramphenicol or phleomycine cassette) and downstream region of the targeted gene was PCR amplified with specific primers (listed in Supplementary Table S2). The three DNA fragments were linked by overlap PCR to obtain a DNA fragment containing the antibiotic marker flanked by the two homologous recombination regions. This latter fragment was introduced into *B. velezensis* GA1 by natural competence induced by nitrogen limitation[61]. Homologous recombination event was selected by chloramphenicol resistance (or phleomycin resistance for double mutants) on LB medium. All gene deletions were confirmed by PCR analysis with the corresponding UpF and DwR specific primers and by the loss of the corresponding BSMs production.

Transformation of the *B. velezensis* GA1 strain was performed following the protocol described by Jarmer et al., [61] with certain modifications. One fresh GA1 colony was inoculated into LB liquid medium at 37°C (160 rpm) until reaching an OD_{600nm} of 1.0. Afterwards, cells were washed one time with peptone water and one time with a modified Spizizen minimal salt medium called MMG liquid medium (19 g l^{-1} K_2HPO_4 anhydrous; 6 g l^{-1} KH_2PO_4; 1 g l^{-1} Na_3 citrate anhydrous; 0.2 g l^{-1} $MgSO_4$ $7H_2O$; 2 g l^{-1} Na_2SO_4; 50 µM $FeCl_3$ (sterilized by filtration at 0.22 µm); 2µM $MnSO_4$; 8 g l^{-1} glucose; 2 g l^{-1} L-glutamic acid; pH 7.0), 1µg of DNA recombinant fragment was added to the GA1 cells suspension adjusted to an OD_{600nm} of 0.01 into MMG liquid medium. One day after incubation at 37°C with shaking at 165 rpm, bacteria were spread on LB plates supplemented with the appropriated antibiotic to select positive colonies.

Construction of deletion mutants of *Pseudomonas* sp. CMR12a

Pyochelin and pyoverdine mutants of *Pseudomonas* sp. CMR12a were constructed using the I-SceI system and the pEMG suicid vector [62,63]. Briefly, the upstream and downstream region flanking the *pchA* (*C4K39_5481*) or the *pvdI* (*C4K39_6027*) genes were PCR amplified (with primers listed in the

Supplementary Table S2), linked via overlap PCR and inserted into the pEMG vector. The resulting plasmid (listed in Supplementary Table S1) was integrated by conjugation into the *Pseudomonas* sp. CMR12a chromosome via homologous recombination. Kanamycin (25µg/mL) resistant cells were selected on King B agar plates and transformed by electroporation with the pSW-2 plasmid (harboring I-SceI system). Gentamycin (20µg/ml) resistant colonies on agar plates were transferred to King B medium with and without kanamycine to verify the loss of the antibiotic (kanamycin) resistance. *Pseudomonas* mutants were identified by PCR with the corresponding UpF and DwR specific primers and via the loss of pyochelin or/and pyoverdin production (see section Secondary metabolites analysis).

Pseudomonas sp. cell-free supernatant

Pseudomonas sp. strains were grown overnight on LB solid medium, at 30°C. Cells were adjusted to OD_{600nm} of 0.05 by resuspension with 100 ml of CAA and when appropriate supplemented with 20 µg/l of $FeCl_3.6H_2O$ (iron supplementation). Cultures were shaken at 120 rpm at 30°C for 48 h and then centrifuged at 5000 rpm at room temperature (22°C) with a Universal 320 centrifuge (Hettich) for 20 min. The supernatant was sterilized with a 0.22 µm pore size Sterile PES Syringe (ROCC S.A.) filters and stored at -20°C until needed.

Dual interaction and time course experiment

B. velezensis strains were grown overnight on LB solid medium, at 30°C. Cells were resuspended in 2 ml of $EM_{1/2}$ liquid medium to a final OD_{600nm} of 0.1 in which 1, 2, 4, or 8% v/v (depending on the experiment) of *Pseudomonas* CFS were added while the control remained without the addition of CFS. *B. velezensis* liquid cultures were shaken in an incubator at 300 rpm at 30°C for 24 h. During the culture time course experiment, at 8, 24, and 36 h, the OD_{600nm} was measured with VWR, V-1200 Spectrophotometer to correlate it with *Pseudomonas* CFS effect on *Bacillus* growth and BSMs production. In addition, 2 ml of the (co-)culture supernatants were sampled, centrifugated at 5000 rpm at room temperature (approx. 22°C) for 10 min to extract supernatants and collect the cells. Cell-free (co-)culture supernatants were obtained by sterilization with a 0.22µm pore size Sterile CA Syringe filters and thus used for analytical analysis of secondary metabolites (as mentioned above) and antibacterial assays. For some experiments using 2H-bae as a marker, the CFS obtained from the double mutant sessilin and orfamide (Δ*sesA-ofaBC*) was used as a control instead of CFS from CMR12a wild-type because it yielded a higher response and lower inhibition interferences by CLPs. The remaining cells after supernatant collection were stored at -80°C to avoid RNA degradation, until performing RT-qPCR analysis.

Antimicrobial activity assays

Antibacterial activity of the *B. velezensis* supernatant generated after dual interaction with *Pseudomonas* CFS was tested against *X. campestris* pv. *campestris* and *C. michiganensis* subsp. *michiganensis.* The activity of co-culture supernatants was quantified in microtiter plates (96-well) filled with 250 µl of LB liquid medium, inoculated at OD_{600nm}= 0.1 with *X. campestris* pv. *campestris* and *C. michiganensis* subsp. *michiganensis* and supplemented with 2% or 6% v/v of *B. velezensis* supernatants, respectively. The activity of (co-)culture supernatants was estimated by measuring the pathogen OD_{600nm} every 30min during 24h with a Spectramax® (Molecular Devices, Wokingham, UK), continuously shaken, at 30°C. For estimating the activity of co-culture supernatants on solid medium, 5 µl supernatantwas applied to a sterile paper disk (5 mm diameter). After drying, diskswere placed on LBAsquare plates previously inoculated with a confluent layer of *X. campestris* pv. *campestris* or *C. michiganensis* subsp. *michiganensis*. LB liquid medium was used as negative control. Plates were incubated at 25°C for 48 h. Three repetitions were done and the inhibition zones from the edge of the paper discs to the edge of the zone were measured.

RNA isolation and RT-qPCR.

RNA extraction and Dnase treatment were carried out using the NucleoSpin RNA Kit (Macherey Nagel, Germany), following the Gram + manufacturer's protocol. RNA quality and quantity were performed with Thermo scientific NanoDrop 2000 UV-vis Spectrophotometer. The gyrase gene was chosen as a housekeeping gene to normalize mRNA levels between different samples. The target gene in this study was *acnA*. Primer 3 program available online was used for primer design and primers were synthesized by Eurogentec. The primer efficiency was evaluated and primer pairs showing an efficiency between 90 and 110% in qPCR analysis were selected. Reverse transcriptase and RT-qPCR reactions were conducted using the Luna® Universal One-Step RT-qPCR Kit (New England Biolabs, Ipswich, MA, United States). The reaction was performed with 50 ng of total RNA in a total volume of 20 µL: 10 µL of luna universal reaction mix, 0.8 µL of each primer (10 µM), 5 µL of cDNA (50ng), 1µL of RT Enzyme MIX, 2.4 µl of Nuclease-free water. The thermal cycling program applied on the ABI StepOne was: 55°c for 10 min, 95C °C for 1 min, 40 cycles of 95 °C for 10 s and 60 °C for 1 min, followed by a melting curve analysis performed using the default program of the ABI StepOne qPCR machine (Applied Biosystems). The real-time PCR amplification was run on the ABI step-one qPCR instrument (Applied Biosystems) with software version 2.3. Analysis was conducted on gene expression level and has been quantified using the $2^{-\Delta\Delta CT}$ method[64].

Secondary metabolite analysis

For detection of BSMs, *B. velezensis* and *Pseudomonas* sp. were cultured in EM and CAA as described above. After an incubation period of 24 h for *B. velezensis*, if not differentially indicated, and 48 h for *Pseudomonas* sp., supernatants of the bacteria were collected and analyzed by UPLC MS/MS and UPLC qTOF MS/MS. Analysis of *Bacillus* metabolites was performed by UPLC MS/MS using an Acquity UPLC® BEH C 18 column (L=50mm, D= 2.1mm, Particles diameter= 1.7µm) (Waters, milford, MA, USA). The volume injected was 10 µl. Mass spectrometer (Acquity UPLC ® Class H SQD (Water, milford, MA, USA)) was set in negative mode ESI- and positive more ES+ (cone voltage: 60V) with a mass range from m/z 300.00 to 2048.00. Analysis of *Pseudomonas* metabolites was performed by Q-TOF (tandem mass spectrometry, quadrupole and Time of flight detector combined) (Agilent, Waldbronn, Germany) and a diode array detector (DAD) 190 to 601 nm (steps: 1nm). The volume injected was 10µl. The mass analysis was performed in positive mode ES+ (Dual AJS ESI) (Vcap= 3500V, Nozzle Voltage= 1000V), with a mass range from m/z 180 to 1700.

Bioguided fractionation

Pseudomonas CFS were concentrated with a C18 cartridge 'Chromafix, small' (Macherey-Nagel, Düren, Germany). The column was conditioned with 10 ml of MeOH followed by 10ml of milliQ water. Then, 20 ml of supernatant flowed through the column. The metabolites were eluted with 1 ml of a solution of increasing acetonitrile/water ratio from 5:95 to 100:0 (v/v). The triggering effect of these fractions on *Bacillus* 2H-bae production was tested in 48 wells microplate containing 1 ml of EM medium inoculated with *B. velezensis* GA1 (OD_{600nm} = 0.1) and 4% v/v of aforementioned *Pseudomonas* fractions, growing for 24h, with shaking at 300 rpm and 30°C. Afterward, the production of 2H-bae was quantified compared to controls and crude supernatant.

Purification of pyochelin and pyoverdine

Pyoverdine and pyochelin were purified in two steps. Firstly, *Pseudomonas* CFS were concentrated with a C18 cartridge (as indicated in section Bioguided fractionation) and eluted with 2 times 2ml of a solution of water and ACN (15 and 30% of ACN (v/v)). Secondly, the fractions were injected on HPLC for purification performed on an Eclipse+ C18 column (L=150mm, D= 3.0mm, Particles diameter 5µm) (Agilent, Waldbronn, Germany). The volume injected was 100 µl. The UV-Vis absorbance was measured with a VWD Agilent technologies 1100 series (G1314A) detector (Agilent, Waldbronn, Germany). The lamp used was a

Deuterium lamp G1314 Var Wavelength Det. (Agilent, Waldbronn, Germany). Two wavelengths were selected: 320 nm, used for the detection of pyochelin, and 380 nm, used for the detection of pyoverdine. The fractions containing the pyoverdine and pyochelin were collected directly at the detector output. Further, the purity of the samples was verified by two detectors, a diode array detector (DAD) 190 to 601 nm (steps: 1nm) and a Q-TOF (tandem mass spectrometry, quadrupole and Time of flight detector combined) (Agilent, Waldbronn, Germany). Electrospray ionization was performed in positive mode (ESI+) (Dual AJS ESI) (Vcap= 3500V, Nozzle Voltage= 1000V), with mass range from m/z 200 to 1500. Finally, the concentration of pyoverdine and pyochelin were estimated by utilization of Beer Lambert law formula, A=Ɛlc (A: absorbance; Ɛ: molar attenuation coefficient or absorptivity of the attenuating species; l: optical path length and c: concentration of molecule). l value for pyochelin and pyoverdine is 1 cm while Ɛ is 4000 $L.mol^{-1}.cm^{-1}$ or 16000 $L.mol^{-1}.cm^{-1}$, respectively [65]. The absorbance was measured with VWR, V-1200 Spectrophotometer, at 320nm (pH=8) for pyochelin and 380nm (pH=5) for pyoverdine[65]. Further, the absorbance value was used for calculating the final concentration. The fragmentation pattern of *Pseudomonas* sp. CMR12a pyoverdine was obtained by UPLC MS/MS analysis of m/z = 1288.5913 ion in positive mode with a fragmentation energy at 75V and compared to the one described in *P. protegens* Pf-5 [1].

Confrontation, white line formation and motility test

For confrontation assays on agar plates*, Bacillus* and *Pseudomonas.* strains were grown overnight in $EM_{1/2}$ and CAA liquid mediums, respectively. After bacterial washing in peptone water and adjustment of OD_{600nm} to 0.1, 5 µl of bacterial suspension was spotted at 1 mm, 5 mm and 7.5 mm distance onto an $EM_{1/2}$ agar plate. For the white line formation experiments, *B. velezensis* line was applied with a cotton stick and 5 µl of *Psuedomonas* sp. cell suspensions were spotted at a 5 mm distance onto CAA agar plates. Plates were incubated at 30 °C and images taken after 24 h. Photographs were captured using CoolPix camera (NiiKKOR 60x WIDE OPTICAL ZOOM EDVR 4.3-258 mm 1:33-6.5), photos were thus proceeded in Adobe Photoshop CC 2019 or by direct edition.

Maldi-FT-ICR MS imaging

Mass spectrometry images were obtained as recently described (Kune et al 2019) using a FT-ICR mass spectrometer (SolariX XR 9.4T, (Bruker Daltonics, Bremen, Germany)) mass calibrated from 200 m/z to 2,300 m/z to reach a mass accuracy of 0.5 ppm. Region of interest from agar microbial colonies were

directly collected from the Petri dish and transferred onto an ITO Glass slide (Bruker, Bremen, Germany), previously covered with double sided conductive carbon tape. The samples were dried under vacuum and covered with an α-cyano-4-hydroxycinnamic acid (HCCA) matrix solution at 5mg/mL (70:30 acetonitrile:water v/v). In total, 60 layers of HCCA matrix were sprayed using the SunCollect instrument (SunChrom, Friedrichsdorf, Germany). FlexImaging 5.0 (Bruker Daltonics, Bremen, Germany) software was used for MALDI MS imaging acquisition, with a pixel step size for the surface raster set to 100 µm.

In planta competition

For *in planta* studies, tomato seeds (*Solanum lycopersicum* var. Moneymaker) were sterilized in 75% ethanol with shaking for 2 min. Subsequently, ethanol was removed and seeds were added to the 50 ml sterilization solution (8.5 ml of 15% bleach, 0.01 g of Tween 80 and 41.5 ml of sterile ultra-pure water) and shaken for 10 min. Seeds were thereafter washed five times with water to eliminate stock solution residues. Further, seeds were placed on square Petri dishes (5 seeds/plate) containing Hoagland solid medium (14 g/l agar, 5 ml stock 1 (EDTA 5,20 mg/l; $FeSO_4x7H_2O$ 3,90 mg/l; H_3B0_3 1,40 mg/l; $MgSO_4x7H_2O$ 513 mg/l; $MnCl_2x4H_2O$ 0,90 mg/l, $ZnSO_4x7H_2O$ 0,10 mg/l; $CuSO_4x5H_2O$ 0,05 mg/l; 1 ml in 50 ml stock 1, $NaMo0_4x2H_2O$ 0,02 mg/l 1 ml in 50 ml stock 1), 5 ml stock 2 (KH_2PO_4 170 mg/l; 5 ml stock 3 : $KN0_3$ 316 mg/l, $Ca(NO_3)_2$ $4H_2O$ 825 mg/l), pH=6,5) and placed in the dark for three days. Afterwards, 6 seeds were inoculated with 2 µl of overnight culture (OD_{600}=0.1) of the appropriate strains (control) or with a mix of *Bacillus* and *Pseudomonas* cells (95:5 ration) (interaction), and grown at 22°C under a 16h/8h night/day cycle with constant light for three days. After the incubation period, to determine bacterial colonization levels, bacteria from roots of six plants per condition were detached from roots by vortexing for 1 min in peptone water solution supplemented with 0.1% of Tween. Serial dilutions were prepared and 200 µl of each were plated onto LBA medium using plating beads. After 24 h of incubation at 30 °C for *Pseudomonas* and at 42°C for *Bacillus*, colonies were counted. Colonization results (six plants *per* strain) were log-transformed and statistically analyzed. Three independent assays were performed with six plants each for *in planta* competition assays. To measure bacterial BSMs production *in planta*, a rectangle part (1 x 2.5 cm) of medium close to the tomato roots was sampled. BSMs were extracted for 15 min, with an acetonitrile (85%)/agar solution (1:1). After centrifugation for 5 min at 4000 rpm, the supernatant was recovered for the UPLC analysis (section Secondary metabolites analysis).

Statistical analysis

Statistical analyses were performed using GraphPad PRISM version 6 software (GraphPad) by using a paired T-test or Mann-Whitney test. For multiple comparisons, one-way ANOVA and Tukey test were used in RStudio 1.1.423 statistical software environment (R Core Team, 2020). Data represent mean ± s.d. of three independent experiments unless stated otherwise. $P < 0.05$ was considered statistically significant.

Figure legends

Figure 1. Enhanced production of BSMs and related anti-*bacterial* activities of *B. velezensis* GA1 as a response to interaction with *Pseudomonas* sp. CMR12a secreted metabolites. a. LCMS extracted ions chromatograms (EIC) illustrating relative abundance of ions corresponding to dihydrobacillaene (**I**), bacillaene (**II**), bacillibactin (**III**), oxydifficidin (**IV**), difficidin (**V**), surfactins (**VI**), macrolactins (**VII**), iturins (**VIII**) and fengycins (**IX**) produced by *B. velezensis* GA1, after 24h growth in CFS-supplemented (2 % v/v) EM medium (blue) compared to un-supplemented control (red). **b**. Production of *B. velezensis* GA1 BSMs co-cultivated with 2 % (v/v) of *Pseudomonas* sp. CMR12a CFS. Fold change equals to 1 is represented as a red line and corresponds to the production of metabolites in *B. velezensis* GA1 unsupplemented. Statistical significance of each condition (n=9 within three biological repetitions and three technical replicates) was calculated as a comparison of BSMs production by *B. velezensis* GA1 in treated cultures with the production in related monoculture, by using Mann–Whitney test where ''****'' represents significant difference (P<0.0001) **c.** Enhanced Anti-*Xanthomonas campestris* (**I** and **II**) and anti-*Clavibacter michiganensis* (**III** and **IV**) activities of *B. velezensis* GA1 after growth in CFS-supplemented (4 %) medium (GA1+CFS) compared to control (GA1) assessed by inhibition zone (**I** and **III**) and liquid pathogens culture growth kinetic (**II** and **IV**) **d.** Anti-*Xanthomonas campestris* (I) and Anti- *Clavibacter michiganensis* (II) activities of *B. velezensis* GA1 (GA1 wt) BSMs and its derived mutants impaired in production of different BSMs. Metabolites not produced by the different mutants are illustrated with red boxes in the table. Error bars indicate standard error (n=6 within two biological repetitions and three technical replicates). Different letters indicate groups of statistically different conditions (one-way ANOVA and Tukey test; P<0.05). **e.** Differential expression of *acnA*, encoding the amylocylicin precusor, upon supplementation with CMR12a CFS compared to control Error bars indicate standard error (n=6 within two biological repetitions and three technical replicates). The statistical difference, in *acnA* gene expression, between the two conditions was calculated by using Mann–Whitney test where ''**'' represents a statistically significant difference between the two conditions (0.001>P<0.05).

Figure 2: Enantio-pyochelin as the main *Pseudomonas* sp. CMR12a triggers of the anti-*bacterial* activity of *B. velezensis* GA1. a, Effect of 2% v/v *Pseudomonas* sp. CMR12a mutants CFS on dihydrobacillaene (2H-bae)

production by *B. velezensis* GA1. Metabolites not produced by the different mutants are illustrated by red boxes in the table below. Fold change equals to 1 is represented as a red line and corresponds to the production of 2H-bae in *B. velezensis* GA1 unsupplemented culture. Error bars indicate standard error (n= 9 with three biological repetitions and three technical replicates). Different letters indicate groups of statistically different conditions (one-way ANOVA and Tukey test; P<0.05). **b,** Differential production of 2H-bae after addition of 0.35µM pure pyoverdine (PVD), 1.4µM pure enantio-pyochelin (PCH), 4% v/v *Pseudomonas* sp. CMR12a cell-free supernatant (CFS CAA) , CMR12a cell-free supernatant from iron supplemented culture (CFS CAA+Fe) and different concentration of iron-chelating agent 2,2'-dipyridyl (DIP). Fold change equals to 1 is represented as a red line and corresponds to the production of 2H-bae in *B. velezensis* GA1 unsupplemented culture. Error bars indicate standard error (n=6 within two biological repetitions and three technical replicates). Different letters indicate groups of statistically different conditions (one-way ANOVA and Tukey test; P-value < 0.05). **c,** Effect of pure PVD and PCH on bacillibactin and 2H-bae production by *B. velezensis* GA1. *B. velezensis* GA1 culture was supplemented with different concentration of pure PVD or pure PCH. Fold change equals to 1 is represented as a red line and corresponds to the production of 2H-bae in *B. velezensis* GA1 unsupplemented culture. Error bars indicate standard error (n=6 within two biological repetitions and three technical replicates). Different letters indicate groups of statistically different conditions (one-way ANOVA and Tukey test; P<0.05). **d.** Growth curve of GA1 WT and bacillibactin KO mutant (ΔdhbC) upon supplementation with pyoverdine (pvd) and pyochelin (pch) at concentration corresponding to the ones in co-culture experiment (4% (v/v)) pseudomonas CFS . Error bars indicate standard error (n=6 with two biological repetitions and three technical replicates).

Figure 3: Enhanced motility of *Bacillus* is driven by distance and surfactin production . a, *B. velezensis* GA1 and P. sp. CMR12a phenotypes when cultured alone (left panel) or in confrontation at short distance (1cm)(right panel). **b,** Phenotype and motile of GA1 in confrontation with CMR12a at short distance (1cm) compared to his surfactin defficient mutant (Δ*srfaA*) **c,** Maldi FT-ICR MSI (Mass spectrometry Imaging) heatmaps showing spatial localisation and relative abundance of C14-Surfactin ($[M+Na]^+$) when *B. velezensis* GA1 is in confrontation with CMR12a at different distances.

Figure 4: Overview of the unsuspected roles of bacterial CLPs in *Bacillus-Pseudomonas* interaction: **a,** Illustration of *B. velezensis* GA1 growth inhibition cultured in gelosed media in confrontation (**I**) or in liquid with 6%v/v (**II**) with *Pseudomonas* sp. CMR12a wild-type (CFS) or mutants devoid of production of orfamides and phenazines (Δ*ofaBC-phz*), sessilins (Δ*sesA*), sessilins and orfamides (Δ*sesA-ofaBC*), sessilins and phenazines (Δ*sesA-phz*), or sessilins, orfamides and phenazines (Δ*sesA-ofaBC-phz*). Error bars indicate standard error (n=6 within two biological repetitions and three technical replicates). Different letters indicate groups of statistically different conditions (one-way ANOVA and Tukey test; P<0.05). **b, Left** : Optical density of B. velezensis GA1 WT (GA1) after 7h culture supplemented with CMR12a WT CFS (CMR12a) or sessilin KO mutant (Δ*sesA*).**Right :** Optical density of B. velezensis GA1 surfactin KO mutant (Δ*srfaA*) after 7h culture supplemented with CMR12a WT CFS (CMR12a) and pure surfactin (CMR12a + surfactin). Growth inhibition of CMR12 sessilin mutant CFS (Δ*sesA*). Unsupplemented culture of both B. velezensis strains are mentioned as control culture**. c-** White line formation obtained by confrontation with surfactin and sessilin/tolaasin producing strains (*B. velezensis* GA1 confronted to *Pseudomonas* sp. CMR12a (**I**) or *P.* tolaasii CH36 (**II**). CLPs impaired mutants (Δ*srfaA,* and Δ*sesA* or Δ*tolA*) do not show any white-line. Other *Pseudomonas* CLPs producers do not cause white-line formation or impact the *B. velezensis* GA1 growth (WCU-84, SS101, BW11M1, RW10S2).. CLPs produced by the aforementioned *Pseudomonas* strains are listed in the table below. **d.** 3D LC-MS chromatogram after solid-liquid extraction of white-line showing the presence of sessilin and surfactin.

Figure 5: *Bacillus-Pseudomonas in planta* competition and CLPs role. **a.** *Bacillus* (GA1) or *Pseudomonas* (CMR12a) population recovered at 3 days post inoculation (dpi) when inoculated alone (GA1, CMR12a) or coinoculated (co-inoculation) . Error bars indicate standard error (n=16) of 3 independent experiments including at least 4 plants per condition. Statistical difference between the conditions was calculated by using Mann–Whitney test where ‘’****’’ and ‘’***’’ represent significant differences (P<0.0001 and 0.0001>P<0.001, respectively). **b.** Relative gene expression of *srfaA, dfnA, baeJ* and *acnA*a fter 3 days of co-inoculation on tomato plant roots. Error bars indicate standard error (n=3, each dot represents the mean of three technical repetitions). Fold change equals to 1 is represented as a red line and corresponds to the gene expressions in *B. velezensis* GA1 monoculture. Statistical significance of each group was calculated as a comparison of genes expressions by *B. velezensis* GA1 in treated cultures with the one in monocultures, by using T-test where ‘’*’’, ‘’***’’ and ‘’****’’ represent significant difference (0.01>P<0.05, 0.0001>P<0.001

and P<0.0001, respectively). **c.** Recoverd population at 3dpi of *B. velezensis* GA1 WT (GA1) or his surfactin impaired mutant (Δ*srfA*) co-inoculatied with *P. sp.* CMR12a (CMR12a) or his sessilin KO mutant (Δ*sesA*) . Error bars represent standard deviations (n=16 to 18) of 3 independent experiments including at least 4 plants per condition. Statistical difference between two conditions was calculated by using Mann–Whitney test where ''**'' indicates a significant difference (0.001>P<0.05). **d.** LC-MS EIC illustrating relative *in planta* production of sessilin and surfactin by monocultures of *B. velezensis* GA1 (GA1) and co-cultures of wild types (GA1+CMR12a) and *B. velezensis* GA1 and *Pseudomonas* sp. CMR12a impaired in sessilin production (GA1+Δsessilin).

Funding

This work was supported by the EU Interreg V France-Wallonie-Vlaanderen portfolio SmartBiocontrol (Bioprotect and Bioscreen projects, avec le soutien du Fonds européen de développement régional - Met steun van het Europees Fonds voor Regionale Ontwikkeling), by the European Union Horizon 2020 research and innovation program under grant agreement No. 731077 and by the EOS project ID 30650620 from the FWO/F.R.S.-FNRS. FB is recipient of a F.R.I.A. fellowship (Formation à la Recherche dans l'Industrie et l'Agriculture) and MO is senior research associate at the F.R.S.-F.N.R.S. We are grateful to the KU Leuven HPC infrastructure and the Flemish Supercomputer Center (VSC) for providing the computational resources and services to perform the RNA-seq analysis. The MALDI FT-ICR SolariX XR were funded by FEDER BIOMED HUB Technology Support (number 2.2.1/996).

Acknowledgments

We gratefully acknowledge Sébastien Rigali, Alexandre Jousset and Loïc Ongena for critically reading the manuscript. We thank C. Keel for the kind gift of strains and J. Vacheron for the very helpful indications on *Pseudomonas* mutagenesis.

REFERENCES

1. Nayfach, S. *et al.* A genomic catalog of Earth's microbiomes. *Nat. Biotechnol.* (2020). doi:10.1038/s41587-020-0718-6
2. Fierer, N. Embracing the unknown: disentangling the complexities of the soil microbiome. *Nat. Rev. Microbiol.* **15**, 579–590 (2017).
3. Schmidt, R., Ulanova, D., Wick, L. Y., Bode, H. B. & Garbeva, P. Microbe-driven chemical ecology: past, present and future. *ISME Journal* **13**, 2656–2663 (2019).
4. Tyc, O., Song, C., Dickschat, J. S., Vos, M. & Garbeva, P. The Ecological Role of Volatile and Soluble Secondary Metabolites Produced by Soil Bacteria. *Trends Microbiol.* **25**, 280–292 (2017).
5. Bernal, P., Llamas, M. A. & Filloux, A. Type VI secretion systems in plant-associated bacteria. *Environ. Microbiol.* **20**, 1–15 (2018).
6. Andrić, S., Meyer, T. & Ongena, M. Bacillus Responses to Plant-Associated Fungal and Bacterial Communities. *Front. Microbiol.* **11**, (2020).
7. Abreu, N. A. & Taga, M. E. Decoding molecular interactions in microbial communitiesa. *FEMS Microbiol. Rev.* **40**, 648–663 (2016).
8. Mendes, R., Garbeva, P. & Raaijmakers, J. M. The rhizosphere microbiome: significance of plant beneficial, plant pathogenic, and human pathogenic microorganisms. *FEMS Microbiol. Rev.* **37**, 634–663 (2013).
9. Müller, D. B., Vogel, C., Bai, Y. & Vorholt, J. A. The Plant Microbiota: Systems-Level Insights and Perspectives. *Annu. Rev. Genet.* **50**, 211–234 (2016).
10. Penha, R. O., Vandenberghe, L. P. S., Faulds, C., Soccol, V. T. & Soccol, C. R. Bacillus lipopeptides as powerful pest control agents for a more sustainable and healthy agriculture: recent studies and innovations. *Planta* **251**, 1–15 (2020).
11. Grubbs, K. J. *et al.* Large-Scale Bioinformatics Analysis of *Bacillus* Genomes Uncovers Conserved Roles of Natural Products in Bacterial Physiology. *mSystems* **2**, 1–18 (2017).
12. Harwood, C. R., Mouillon, J.-M. M., Pohl, S. & Arnau, J. Secondary metabolite production and the safety of industrially important members of the Bacillus subtilis group. *FEMS Microbiol. Rev.* **42**, 721–738 (2018).
13. Ye, M. *et al.* Characteristics and Application of a Novel Species of *Bacillus* : *Bacillus velezensis*. *ACS Chem. Biol.* **13**, 500–505 (2018).
14. Rabbee, M. *et al. Bacillus velezensis*: A Valuable Member of Bioactive Molecules within Plant Microbiomes. *Molecules* **24**, 1–13 (2019).

642 15. Pieterse, C. M. J. *et al.* Induced Systemic Resistance by Beneficial Microbes. *Annu. Rev. Phytopathol.*
643 **52**, 347–375 (2014).
644 16. Köhl, J., Kolnaar, R. & Ravensberg, W. J. Mode of Action of Microbial Biological Control Agents
645 Against Plant Diseases: Relevance Beyond Efficacy. *Front. Plant Sci.* **10**, 845 (2019).
646 17. Traxler, M. F. & Kolter, R. Natural products in soil microbe interactions and evolution. *Nat. Prod. Rep.*
647 **32**, 956–970 (2015).
648 18. Raaijmakers, J. M. & Mazzola, M. Diversity and Natural Functions of Antibiotics Produced by
649 Beneficial and Plant Pathogenic Bacteria. *Annu. Rev. Phytopathol.* **50**, 403–424 (2012).
650 19. Li, Y. & Rebuffat, S. The manifold roles of microbial ribosomal peptide-based natural products in
651 physiology and ecology. *J. Biol. Chem.* **295**, 34–54 (2020).
652 20. Arguelles Arias, A. *et al.* Characterization of Amylolysin, a Novel Lantibiotic from Bacillus
653 amyloliquefaciens GA1. *PLoS One* **8**, e83037 (2013).
654 21. Scholz, R. *et al.* Amylocyclicin, a novel circular bacteriocin produced by Bacillus amyloliquefaciens
655 FZB42. *J. Bacteriol.* **196**, 1842–1852 (2014).
656 22. Torres Manno, M. A. *et al.* GeM-Pro: a tool for genome functional mining and microbial profiling.
657 *Appl. Microbiol. Biotechnol.* **103**, 3123–3134 (2019).
658 23. Dutta, S. *et al.* Structure of a modular polyketide synthase. *Nature* **510**, 512–517 (2014).
659 24. Winn, M., Fyans, J. K., Zhuo, Y. & Micklefield, J. Recent advances in engineering nonribosomal
660 peptide assembly lines. *Nat. Prod. Rep.* **33**, 317–347 (2016).
661 25. Bozhüyük, K. A., Micklefield, J. & Wilkinson, B. Engineering enzymatic assembly lines to produce new
662 antibiotics. *Curr. Opin. Microbiol.* **51**, 88–96 (2019).
663 26. Zhao, X. & Kuipers, O. P. O. P. Identification and classification of known and putative antimicrobial
664 compounds produced by a wide variety of Bacillales species. *BMC Genomics* **17**, (2016).
665 27. Raaijmakers, J. M., de Bruijn, I., Nybroe, O. & Ongena, M. Natural functions of lipopeptides from
666 Bacillus and Pseudomonas: More than surfactants and antibiotics. *FEMS Microbiol. Rev.* **34**, 1037–
667 1062 (2010).
668 28. Blin, K. *et al.* antiSMASH 5.0: updates to the secondary metabolite genome mining pipeline. *Nucleic*
669 *Acids Res.* **47**, W81–W87 (2019).
670 29. Nihorimbere, V. *et al.* Impact of rhizosphere factors on cyclic lipopeptide signature from the plant
671 beneficial strain Bacillus amyloliquefaciens S499. *FEMS Microbiol. Ecol.* **79**, 176–191 (2012).
672 30. D'aes, J. *et al.* To settle or to move? The interplay between two classes of cyclic lipopeptides in the

673 biocontrol strain Pseudomonas CMR12a. *Environ. Microbiol.* **16**, 2282–2300 (2014).
674 31. Hua, G. K. H. & Höfte, M. The involvement of phenazines and cyclic lipopeptide sessilin in biocontrol
675 of Rhizoctonia root rot on bean (Phaseolus vulgaris) by Pseudomonas sp. CMR12a is influenced by
676 substrate composition. *Plant Soil* **388**, 243–253 (2015).
677 32. Perneel, M. *et al.* Characterization of CMR5c and CMR12a, novel fluorescent Pseudomonas strains
678 from the cocoyam rhizosphere with biocontrol activity. *J. Appl. Microbiol.* **103**, 1007–1020 (2007).
679 33. Olorunleke, F. E. *et al.* Coregulation of the cyclic lipopeptides orfamide and sessilin in the biocontrol
680 strain Pseudomonas sp. CMR12a. *Microbiologyopen* **6**, 1–12 (2017).
681 34. Olorunleke, F. E., Hua, G. K. H., Kieu, N. P., Ma, Z. & Höfte, M. Interplay between orfamides, sessilins
682 and phenazines in the control of Rhizoctonia diseases by Pseudomonas sp. CMR12a. *Environ.*
683 *Microbiol. Rep.* **7**, 774–781 (2015).
684 35. Geudens, N. & Martins, J. C. Cyclic lipodepsipeptides from Pseudomonas spp. - Biological Swiss-Army
685 knives. *Front. Microbiol.* **9**, 1–18 (2018).
686 36. Omoboye, O. O. *et al.* Pseudomonas cyclic lipopeptides suppress the rice blast fungus Magnaporthe
687 oryzae by induced resistance and direct antagonism. *Front. Plant Sci.* **10**, 901 (2019).
688 37. Mansfield, J. *et al.* Top 10 plant pathogenic bacteria in molecular plant pathology. *Mol. Plant Pathol.*
689 **13**, 614–629 (2012).
690 38. Molinatto, G. *et al.* Complete genome sequence of Bacillus amyloliquefaciens subsp. plantarum
691 S499, a rhizobacterium that triggers plant defences and inhibits fungal phytopathogens. *J.*
692 *Biotechnol.* **238**, 56–59 (2016).
693 39. Fan, B. *et al.* Bacillus velezensis FZB42 in 2018: The gram-positive model strain for plant growth
694 promotion and biocontrol. *Front. Microbiol.* **9**, 3389 (2018).
695 40. Pandin, C. *et al.* Complete genome sequence of Bacillus velezensis QST713: A biocontrol agent that
696 protects Agaricus bisporus crops against the green mould disease. *J. Biotechnol.* **278**, 10–19 (2018).
697 41. Youard, Z. A., Mislin, G. L. A., Majcherczyk, P. A., Schalk, I. J. & Reimmann, C. Pseudomonas
698 fluorescens CHA0 produces enantio-pyochelin, the optical antipode of the pseudomonas aeruginosa
699 siderophore pyochelin. *J. Biol. Chem.* **282**, 35546–35553 (2007).
700 42. Grandchamp, G. *et al.* Pirated siderophores promote sporulation in Bacillus subtilis . *Appl. Environ.*
701 *Microbiol.* **83**, 1–17 (2017).
702 43. Miethke, M. *et al.* Ferri-bacillibactin uptake and hydrolysis in Bacillus subtilis. *Mol. Microbiol.* **61**,
703 1413–1427 (2006).

704 44. Adler, C. *et al.* Catecholate Siderophores Protect Bacteria from Pyochelin Toxicity. *PLoS One* **7**,
705 (2012).
706 45. Trottmann, F., Franke, J., Ishida, K., García-Altares, M. & Hertweck, C. A Pair of Bacterial
707 Siderophores Releases and Traps an Intercellular Signal Molecule: An Unusual Case of Natural
708 Nitrone Bioconjugation. *Angew. Chemie* **131**, 206–210 (2019).
709 46. Hartney, S. L. *et al.* Ferric-pyoverdine recognition by Fpv outer membrane proteins of pseudomonas
710 protegens pf-5. *J. Bacteriol.* **195**, 765–776 (2013).
711 47. Youard, Z. A., Wenner, N. & Reimmann, C. Iron acquisition with the natural siderophore enantiomers
712 pyochelin and enantio-pyochelin in Pseudomonas species. *BioMetals* **24**, 513–522 (2011).
713 48. Rokni-Zadeh, H. *et al.* Genetic and functional characterization of cyclic lipopeptide white-line-
714 inducing principle (WLIP) production by rice rhizosphere isolate pseudomonas putida RW10S2. *Appl.*
715 *Environ. Microbiol.* **78**, 4826–4834 (2012).
716 49. Buyer, J. S., Wright, J. M. & Leong, J. Structure of Pseudobactin A214, a Siderophore from a Bean-
717 Deleterious Pseudomonas. *Biochemistry* **25**, 5492–5499 (1986).
718 50. van Gestel, J., Vlamakis, H. & Kolter, R. From Cell Differentiation to Cell Collectives: Bacillus subtilis
719 Uses Division of Labor to Migrate. *PLoS Biol.* **13**, 1–29 (2015).
720 51. Munsch, P. & Alatossava, T. The white-line-in-agar test is not specific for the two cultivated
721 mushroom associated pseudomonads, Pseudomonas tolaasii and Pseudomonas 'reactans'.
722 *Microbiol. Res.* **157**, 7–11 (2002).
723 52. Salari, F. *et al.* Draft Genome Sequence of Pseudomonas aeruginosa Strain LMG 1272, an Atypical
724 White Line Reaction Producer. *Microbiol. Resour. Announc.* **9**, (2020).
725 53. Xu, Z. *et al.* Antibiotic Bacillomycin D Affects Iron Acquisition and Biofilm Formation in Bacillus
726 velezensis through a Btr-Mediated FeuABC-Dependent Pathway. *Cell Rep.* **29**, 1192-1202.e5 (2019).
727 54. Powers, M. J., Sanabria-Valentín, E., Bowers, A. A. & Shank, E. A. Inhibition of cell differentiation in
728 Bacillus subtilis by Pseudomonas protegens. *J. Bacteriol.* **197**, 2129–2138 (2015).
729 55. Molina-Santiago, C. *et al.* The extracellular matrix protects Bacillus subtilis colonies from
730 Pseudomonas invasion and modulates plant co-colonization. *Nat. Commun.* **10**, (2019).
731 56. Liu, Y., Kyle, S. & Straight, P. D. Antibiotic Stimulation of a Bacillus subtilis Migratory Response.
732 *mSphere* **3**, 1–13 (2018).
733 57. Rosenberg, G. *et al.* Not so simple, not so subtle: The interspecies competition between Bacillus
734 simplex and Bacillus subtilis and its impact on the evolution of biofilms. *npj Biofilms Microbiomes* **2**,

735 15027 (2016).

736 58. Straight, P. D., Willey, J. M. & Kolter, R. Interactions between Streptomyces coelicolor and Bacillus
737 subtilis: Role of surfactants in raising aerial structures. *J. Bacteriol.* **188**, 4918–4925 (2006).

738 59. Molina-Santiago, C. *et al.* The extracellular matrix protects Bacillus subtilis colonies from
739 Pseudomonas invasion and modulates plant co-colonization. *Nat. Commun.* **10**, 1919 (2019).

740 60. Lee, N. *et al.* Iron competition triggers antibiotic biosynthesis in Streptomyces coelicolor during
741 coculture with Myxococcus xanthus. *ISME J.* (2020). doi:10.1038/s41396-020-0594-6

742 61. Jarmer, H., Berka, R., Knudsen, S. & Saxild, H. H. Transcriptome analysis documents induced
743 competence of *Bacillus subtilis* during nitrogen limiting conditions. *FEMS Microbiol. Lett.* **206**, 197–
744 200 (2002).

745 62. Martínez-García, E. & de Lorenzo, V. Engineering multiple genomic deletions in Gram-negative
746 bacteria: analysis of the multi-resistant antibiotic profile of Pseudomonas putida KT2440. *Environ.*
747 *Microbiol.* **13**, 2702–2716 (2011).

748 63. Vacheron, J. *et al.* T6SS contributes to gut microbiome invasion and killing of an herbivorous pest
749 insect by plant-beneficial Pseudomonas protegens. *ISME J.* **13**, 1318–1329 (2019).

750 64. Livak, K. J. & Schmittgen, T. D. Analysis of relative gene expression data using real-time quantitative
751 PCR and the 2-ΔΔCT method. *Methods* **25**, 402–408 (2001).

752 65. Hoegy, F., Mislin, G. L. A. & Schalk, I. J. Pyoverdine and pyochelin measurements. *Methods Mol. Biol.*
753 **1149**, 293–301 (2014).

754 66. R Core Team (2020). R: A language and environment for statistical computing. R Foundation for
755 Statistical Computing, Vienna, Austria. (2020). Available at: https://www.r-project.org/.

756

Figure 1

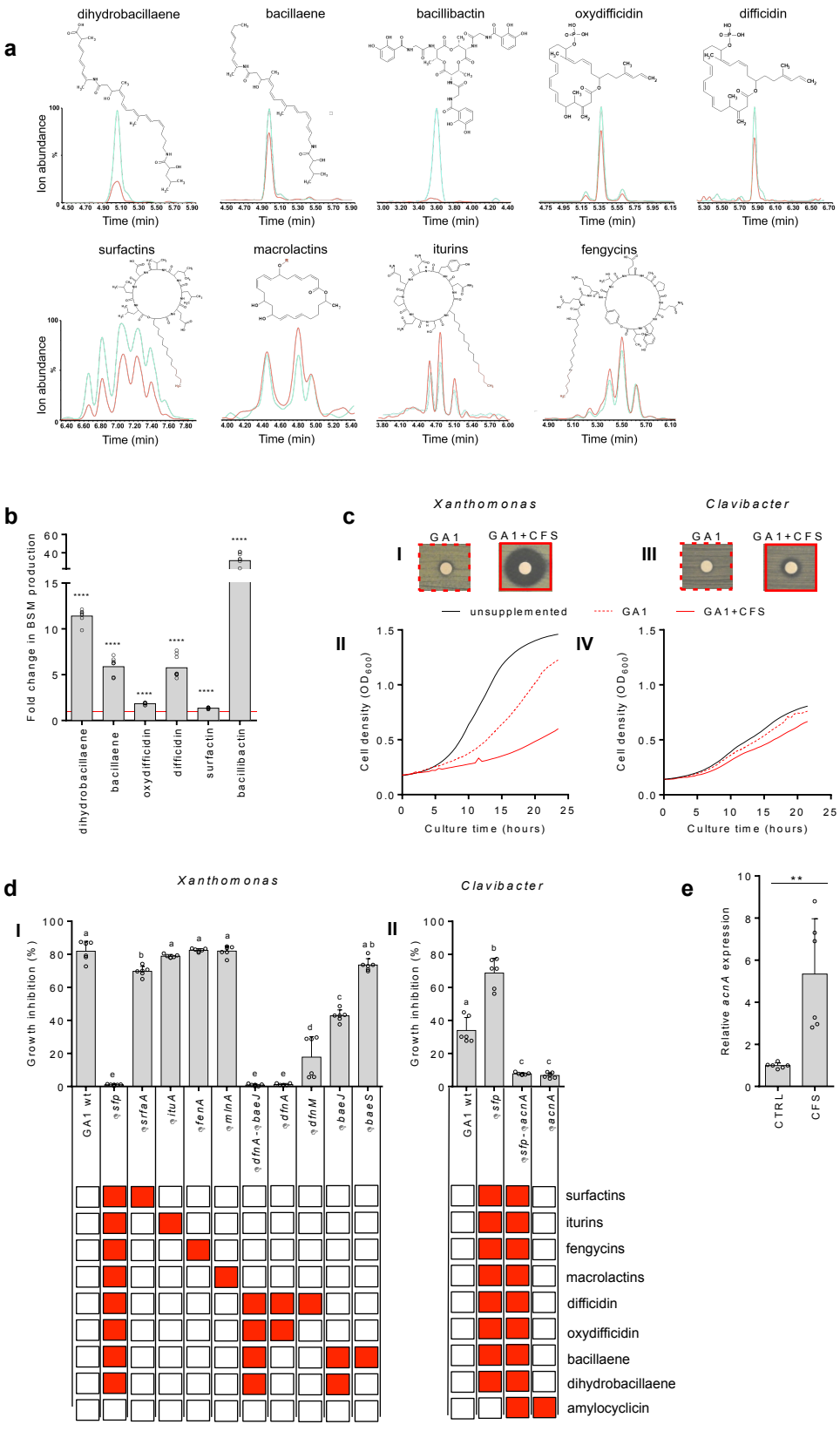
a
dihydrobacillaene
bacillaene
bacillibactin
oxydifficidin
difficidin
surfactins
macrolactins
iturins
fengycins
Ion abundance
Time (min)
b
Fold change in BSM production
dihydrobacillaene
bacillaene
oxydifficidin
difficidin
surfactin
bacillibactin
c
Xanthomonas
Clavibacter
GA1
GA1+CFS
unsupplemented
Cell density (OD600)
Culture time (hours)
d
Xanthomonas
Clavibacter
Growth inhibition (%)
GA1 wt
Δsfp
ΔsrfaA
ΔituA
ΔfenA
ΔmlnA
ΔdfnA-baeJ
ΔdfnA
ΔdfnM
ΔbaeJ
ΔbaeS
Δsfp-acnA
ΔacnA
surfactins
iturins
fengycins
macrolactins
difficidin
oxydifficidin
bacillaene
dihydrobacillaene
amylocyclicin
e
Relative acnA expression
CTRL
CFS

Figure 2

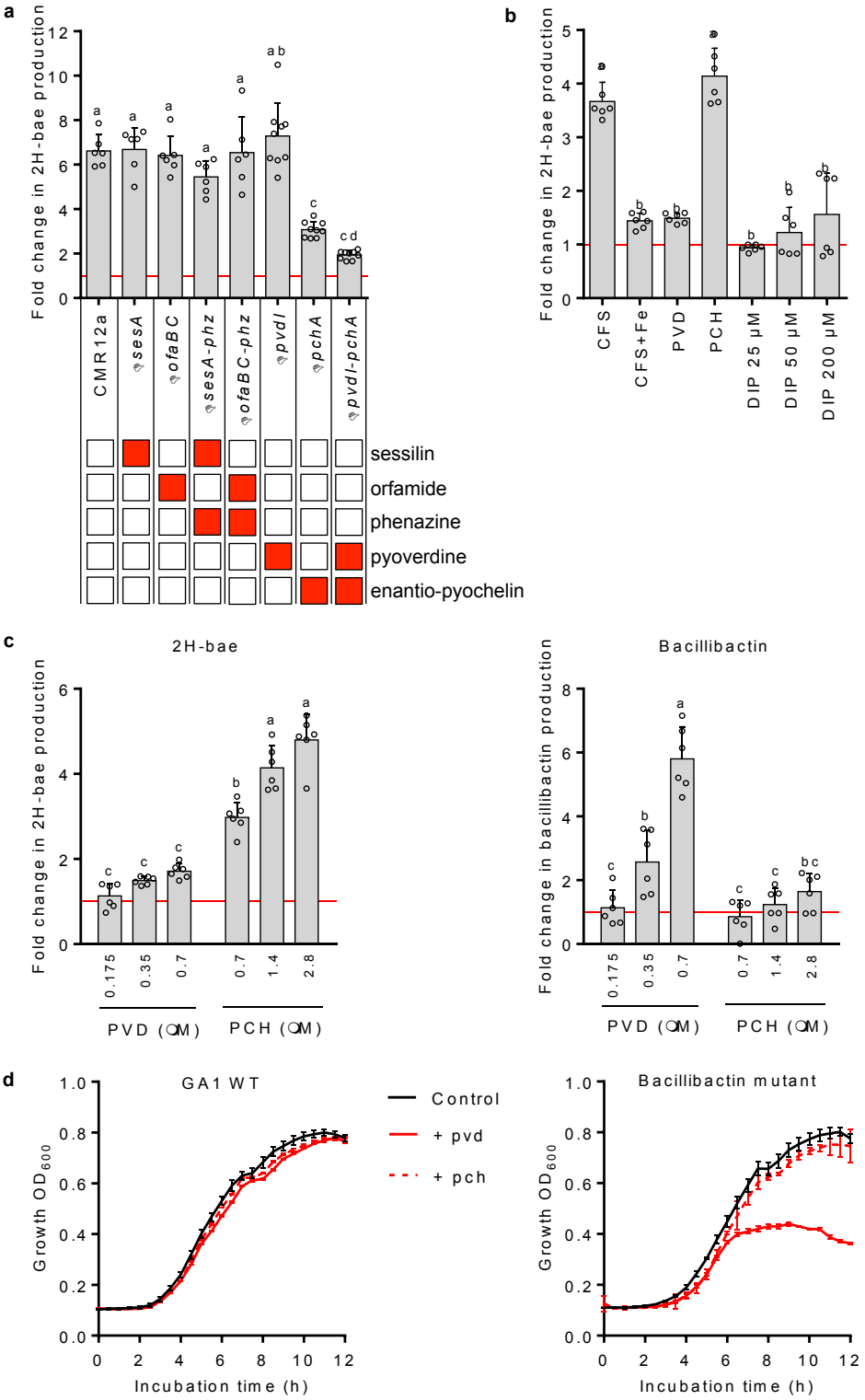
a
Fold change in 2H-bae production
CMR12a
sesA
ofaBC
sesA-phz
ofaBC-phz
pvdI
pchA
pvdI-pchA
sessilin
orfamide
phenazine
pyoverdine
enantio-pyochelin
b
Fold change in 2H-bae production
CFS
CFS+Fe
PVD
PCH
DIP 25 µM
DIP 50 µM
DIP 200 µM
c
2H-bae
Fold change in 2H-bae production
PVD (µM)
PCH (µM)
Bacillibactin
Fold change in bacillibactin production
d
GA1 WT
Bacillibactin mutant
Growth OD600
Incubation time (h)
Control
+ pvd
+ pch

Figure 3

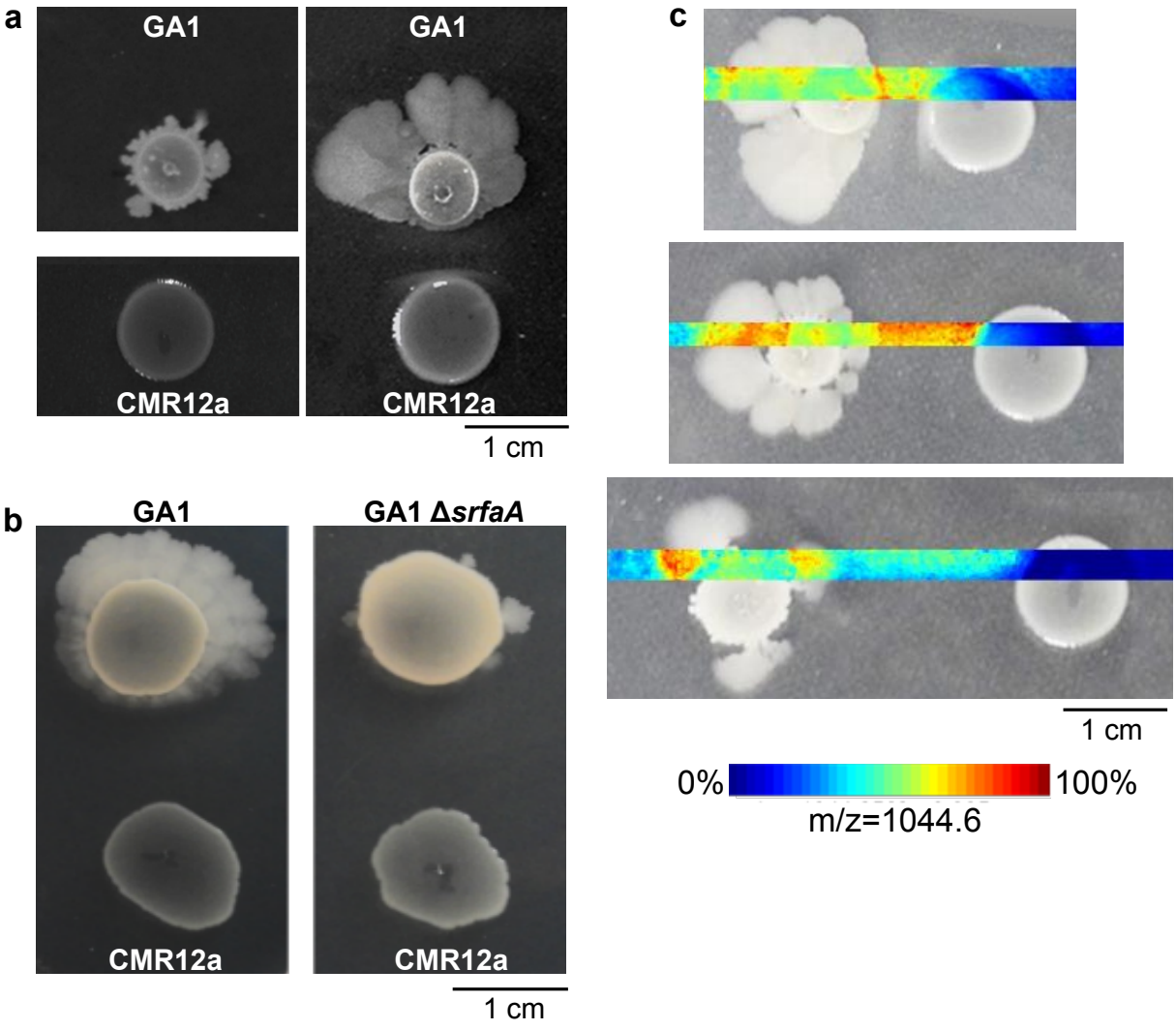
a
GA1
GA1
CMR12a
CMR12a
1 cm
b
GA1
GA1 ΔsrfaA
CMR12a
CMR12a
1 cm
c
1 cm
0%
100%
m/z=1044.6

Figure 4

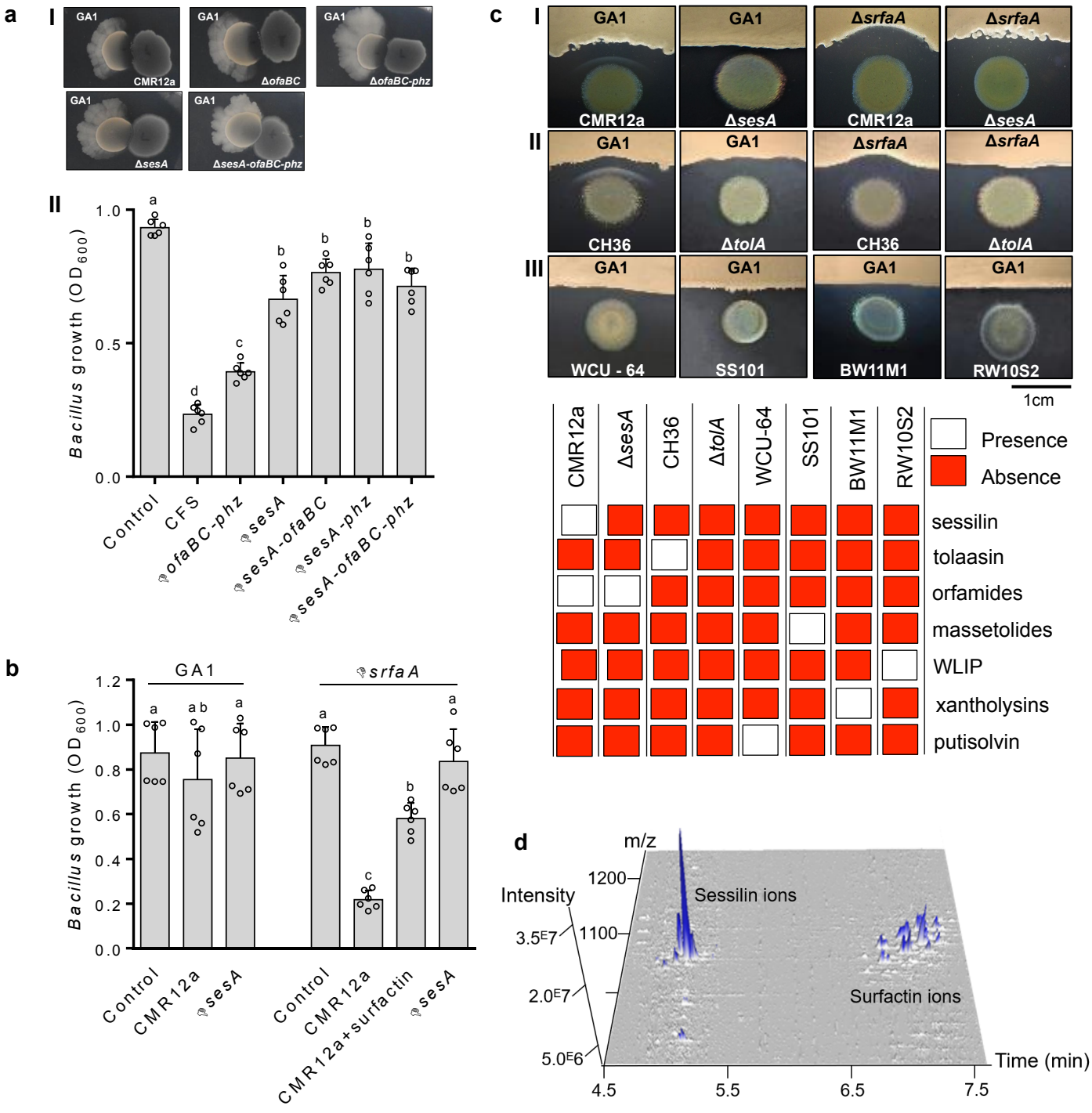
a
I
GA1
CMR12a
ΔofaBC
ΔofaBC-phz
ΔsesA
ΔsesA-ofaBC-phz
II
Bacillus growth (OD600)
Control
CFS
ΔofaBC-phz
ΔsesA
ΔsesA-ofaBC
ΔsesA-phz
ΔsesA-ofaBC-phz
b
GA1
ΔsrfaA
Control
CMR12a
ΔsesA
CMR12a+surfactin
c
I
GA1
ΔsrfaA
CMR12a
ΔsesA
II
CH36
ΔtolA
III
WCU - 64
SS101
BW11M1
RW10S2
1cm
Presence
Absence
sessilin
tolaasin
orfamides
massetolides
WLIP
xantholysins
putisolvin
d
m/z
Intensity
Sessilin ions
Surfactin ions
Time (min)

Figure 5

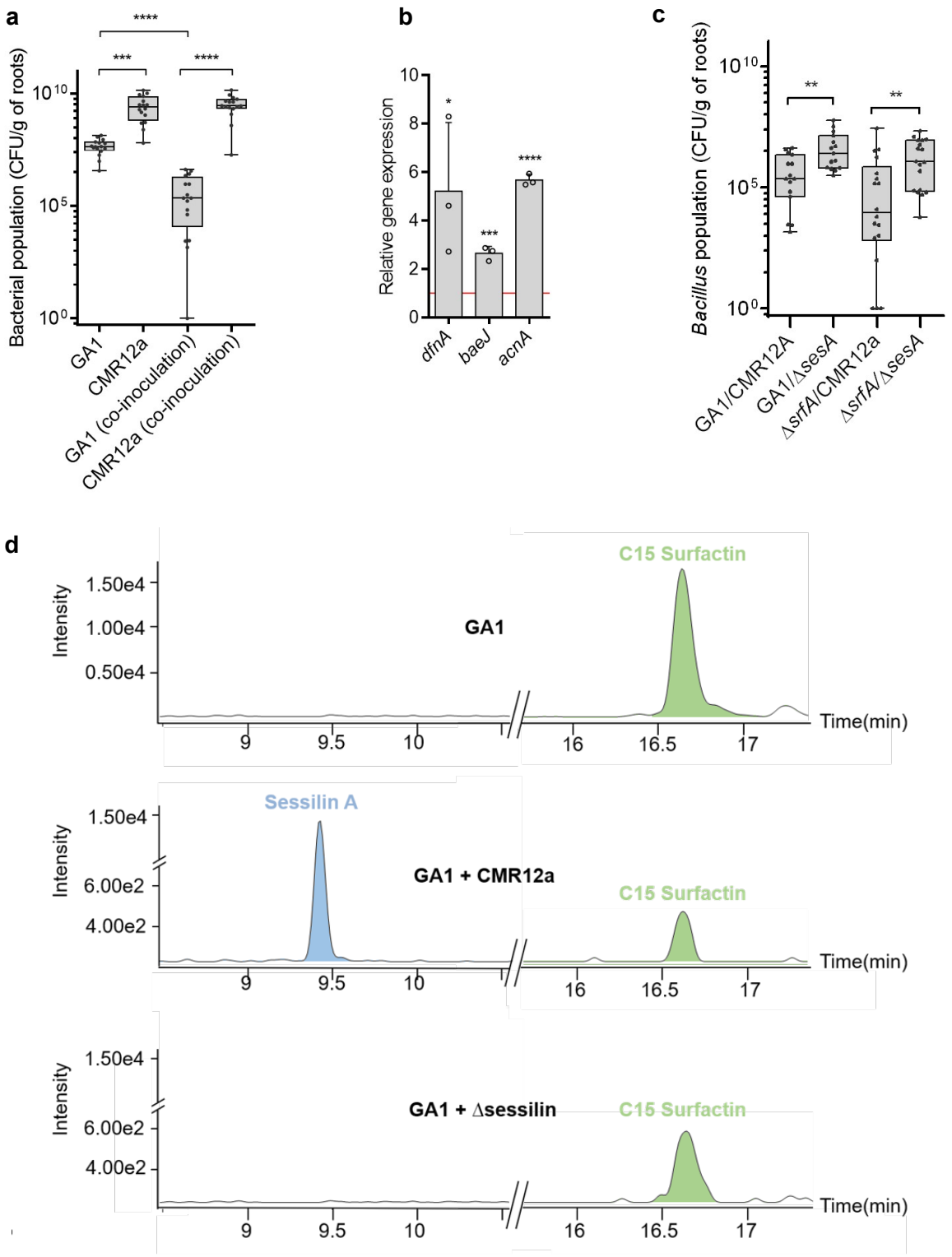
a
b
c
d
Bacterial population (CFU/g of roots)
GA1
CMR12a
GA1 (co-inoculation)
CMR12a (co-inoculation)
Relative gene expression
dfnA
baeJ
acnA
Bacillus population (CFU/g of roots)
GA1/CMR12A
GA1/ΔsesA
ΔsrfA/CMR12a
ΔsrfA/ΔsesA
Intensity
GA1
C15 Surfactin
Time(min)
Sessilin A
GA1 + CMR12a
GA1 + Δsessilin